

1 Supplementary Information for

2

3 **Stimulation of soil respiration by elevated CO<sub>2</sub> is enhanced under nitrogen limitation**

4 **in a decade-long grassland study**

5

6 Qun Gao<sup>a#</sup>, Gangsheng Wang<sup>b#</sup>, Kai Xue<sup>b,c</sup>, Yunfeng Yang<sup>a\*</sup>, Jianping Xie<sup>b,d</sup>, Hao Yu<sup>b,e,f</sup>,

7 Shijie Bai<sup>b,g</sup>, Feifei Liu<sup>b,h</sup>, Zhili He<sup>b,i</sup>, Daliang Ning<sup>b</sup>, Sarah E Hobbie<sup>j</sup>, Peter B Reich<sup>k,l</sup> and

8 Jizhong Zhou<sup>a,b,m\*</sup>

9

10 **\*Corresponding authors:** Dr. Yunfeng Yang; E-mail: [yangyf@tsinghua.edu.cn](mailto:yangyf@tsinghua.edu.cn);

11 Dr. Jizhong Zhou; E-mail: [jzhou@ou.edu](mailto:jzhou@ou.edu)

12

13 <sup>#</sup>The authors contribute equally to this manuscript

14

15 **This PDF file includes:**

16 Supplementary text

17 Figures S1 to S3

18 Tables S1 to S15

19 SI References

20

## 21 **Supplementary Information Text**

### 22 **Detailed modeling methods**

23 **a. Data sources.** Daily GPP values were obtained from a corrected 8-day GPP product  
24 based on the MODIS GPP (MOD17A2/MOD17A2H) (1) and used for the model  
25 simulation of the aCaN plots. We calculated the sum of aboveground plant biomass and  
26 ingrowth root biomass to estimate the net primary production (NPP) (2) for each plot and  
27 averaged NPP across plots for each treatment. The ratio of the averaged NPP of each  
28 treatment relative to that in the control (aCaN) was calculated and was multiplied to the  
29 MODIS GPP values to obtain the daily GPP values of eCaN, aCeN, and eCeN treatments,  
30 considering that there is generally a linear relationship between NPP and GPP (3).  
31 Meanwhile, data sets measured in four CO<sub>2</sub> and N treatment plots across all years were  
32 also used for model simulations, including soil temperature and moisture and the soil CO<sub>2</sub>  
33 efflux.

34

35 **b. C-only TECO model.** The non-microbial C-only terrestrial ecosystem (TECO) model  
36 is a variant of the CENTURY model (4) that is designed to simulate C input from  
37 photosynthesis, C transfer among plant and soil pools, and respiratory C releases to the  
38 atmosphere (Fig. S2b). C dynamics in the TECO model can be described by a group of  
39 first-order ordinary differential equations, where the C turnover rates are modified by soil  
40 temperature ( $T$ ) and moisture ( $W$ ) (5). We assumed that the C turnover rate was distributed  
41 uniformly in a range. We used the Shuffled Complex Evolution (SCE) algorithm (6-8) to  
42 determine model parameters. We also applied the probabilistic inversion (Markov Chain

43 Monte Carlo) to quantify parameter uncertainties (9). By performing TECO modeling,  
44 daily soil CO<sub>2</sub> efflux was simulated for four CO<sub>2</sub> and N treatments from 1998 to 2009.

45

### 46 **c. C-N coupled Microbial-ENzyme Decomposition (MEND) model**

47 **c.1. MEND model description.** We developed a new version of the Microbial-ENzyme  
48 Decomposition (MEND) model, i.e., the C-N coupled MEND model (Fig. S2a), which is  
49 an improvement over the C-only MEND model by incorporating both N cycling processes  
50 and microbial functional traits. The C-only MEND describes SOM decomposition  
51 processes by explicitly representing relevant microbial and enzymatic physiology (8). The  
52 SOM pool consists of two particulate organic matter (POM) pools and one mineral-  
53 associated organic matter (MOM) pool. The two POM pools are decomposed by oxidative  
54 and hydrolytic enzymes, respectively. The MOM is decomposed by enzymes EM. The C-  
55 N coupled MEND model represents additional C-N transformation processes: soil organic  
56 N (SON) decomposition following the SOC decomposition, N mineralization and  
57 immobilization by microbes, nitrification, denitrification, and nitrifier denitrification (10).  
58 In contrast to traditional models that use fixed SOM C:N ratios (11, 12), we use flexible  
59 stoichiometry (i.e., time-variant C:N ratio) for SOM and microbial biomass pools to more  
60 realistically represent the adaption of microbes in response to the stoichiometric imbalance  
61 of available resources (13). Model state variables, governing equations, component fluxes,  
62 and parameters are described in Table S14–S17, respectively. A model parameter (reaction  
63 rate) in MEND may be modified by soil moisture, temperature, or pH (8). MEND  
64 represents nitrification, denitrification, microbial dormancy, resuscitation, mortality, and  
65 enzymatic decomposition in response to changes in moisture, as well as shifting of

66 microbial and enzymatic activities with changing temperature (14). MEND simulates soil  
67 CO<sub>2</sub> efflux ( $R_s$ ) as the sum of autotrophic (root) respiration ( $R_a$ ) and heterotrophic  
68 (microbial) respiration ( $R_h$ ) fluxes:

$$69 \quad R_s = R_a + R_h \quad (1a)$$

$$70 \quad R_a = f_{Ra} \times GPP \quad (1b)$$

$$71 \quad R_h = R_{h,g} + R_{h,m} + R_{h,o} \quad (1c)$$

72 where  $R_a$  is calculated as a fraction ( $f_{Ra} \in (0.1,0.4)$ ) of gross primary production ( $GPP$ , g  
73 C m<sup>-2</sup> d<sup>-1</sup>); and  $R_h$  is the sum of microbial growth ( $R_{h,g}$ ), maintenance ( $R_{h,m}$ ), and overflow  
74 ( $R_{h,o}$ ) respiration fluxes (see Eq. S11 in Table S13 and Eqs. S27–S31 in Table S14).

75

76 **c.2. Model Parameterization.** The model parameters were determined by achieving high  
77 goodness-of-fit of model simulations against experimental observations, such as  $R_s$ ,  
78 concentrations of ammonium (NH<sub>4</sub><sup>+</sup>) and nitrate (NO<sub>3</sub><sup>-</sup>), relative abundances of genes  
79 encoding oxidative (EnzCo) and hydrolytic enzymes (EnzCh) in this study (Table S11).  
80 We implemented multi-objective calibration of the model (6, 14). Each objective evaluates  
81 the goodness-of-fit of a specific observed variable, e.g.,  $R_s$ , or relative gene abundances  
82 (Table S11). Note that the GeoChip gene abundances were used to constrain the MEND  
83 modeling as additional objective functions. The parameter optimization is to minimize the  
84 overall objective function ( $J$ ) that is computed as the weighted average of multiple single-  
85 objectives (Table S15) (15)

$$86 \quad J = \sum_{i=1}^m w_i \cdot J_i \quad (2)$$

$$87 \quad \sum_{i=1}^m w_i = 1 \text{ with } w_i \in [0,1] \quad (3)$$

88 where  $m$  denotes the number of objectives and  $w_i$  is the weighting factor for the  $i^{\text{th}}$  ( $i =$   
 89  $1, 2, \dots, m$ ) objective ( $J_i$ ). In this study,  $J_i$  ( $i=1, 2, \dots, m$ ) refers to the objective function value  
 90 for  $R_s$ , EnzCo and EnzCh, respectively.

91 As the overall objective function  $J$  is minimized in the parameter optimization  
 92 process, the individual objective function  $J_i$  may be calculated as  $(1 - R^2)$ ,  $MARE$ ,  $|PBIAS|$   
 93 (absolute value of  $PBIAS$ ):

$$94 \quad R^2 = 1 - \frac{\sum_{i=1}^n [Y_{sim}(i) - Y_{obs}(i)]^2}{\sum_{i=1}^n [Y_{obs}(i) - \bar{Y}_{obs}]^2} \quad (4)$$

$$95 \quad MARE = \frac{1}{n} \sum_{i=1}^n \left| \frac{Y_{sim}(i) - Y_{obs}(i)}{Y_{obs}(i)} \right| \quad (5)$$

$$96 \quad |PBIAS| = \left| \frac{\bar{Y}_{sim} - \bar{Y}_{obs}}{\bar{Y}_{obs}} \right| \times 100\% \quad (6)$$

97 where  $R^2$  denotes the Coefficient of Determination (16). The  $R^2$  quantifies the proportion  
 98 of the variance in the response variables that is predictable from the independent variables.  
 99 A higher  $R^2$  ( $R^2 \leq 1$ ) indicates better model performance.  $MARE$  is the Mean Absolute  
 100 Relative Error (MARE), and lower  $MARE$  values ( $MARE \geq 0$ ) are preferred (17).  $MARE$   
 101 represents the averaged deviations of predictions ( $Y_{sim}$ ) from their observations ( $Y_{obs}$ ).  
 102  $PBIAS$  is the percent bias between simulated and observed mean values (18).  $n$  is the  
 103 number of data;  $Y_{obs}$  and  $Y_{sim}$  are observed and simulated values, respectively; and  $\bar{Y}_{obs}$  and  
 104  $\bar{Y}_{sim}$  are the mean value for  $Y_{obs}$  and  $Y_{sim}$ , respectively.

105 Different objective functions are used to quantify the goodness-of-fit for different  
 106 variables (Table S15), depending on the measurement method and frequency of variables.  
 107 The coefficient of determination ( $R^2$ ) (16) is used to evaluate the variables (e.g., soil  $\text{CO}_2$   
 108 efflux) that are frequently measured, and the absolute values can be directly compared

109 between observations and simulations. The *MARE* or *PBIAS* is used to evaluate the  
110 variables (e.g., microbial biomass and enzyme concentrations) with only a few  
111 measurements, and the absolute values can be directly compared.

112 We used the modified Shuffled Complex Evolution (SCE) algorithm (6, 7) to calibrate  
113 model parameters for the aCO<sub>2</sub>-aN plots. We then validated the model by using the same  
114 set of model parameters calibrated for aCO<sub>2</sub>-aN to simulate  $R_h$  and  $R_s$ , enzyme  
115 concentration, and soil mineral N in the eCO<sub>2</sub>-aN, aCO<sub>2</sub>-eN, and eCO<sub>2</sub>-eN treatment plots.  
116 Model simulations for each treatment were driven by the corresponding data: GPP, soil  
117 temperature, soil moisture, and soil mineral N (NH<sub>4</sub><sup>+</sup> and NO<sub>3</sub><sup>-</sup>) input.

118

119 **c.3. Uncertainty quantification.** The parameter uncertainty in the MEND model was  
120 quantified by the Critical Objective Function Index (COFI) method (8). The COFI method  
121 is based on a global stochastic optimization technique (e.g., SCE in this study). It also  
122 accounts for model complexity (represented by the number of model parameters) and  
123 observational data availability (represented by the number of observations). The  
124 confidence region of parametric space was determined by selecting those parameter sets  
125 resulting in objective function values ( $J$ ) less than the COFI value ( $J_{cr}$ ) from the feasible  
126 parameter space (8). We used the coefficient of variation (CV) to quantify the uncertainty  
127 for 10 calibrated model parameters. The CV values of all calibrated parameters of gMEND,  
128 tMEND, and TECO were compared (Fig. 3b).

129

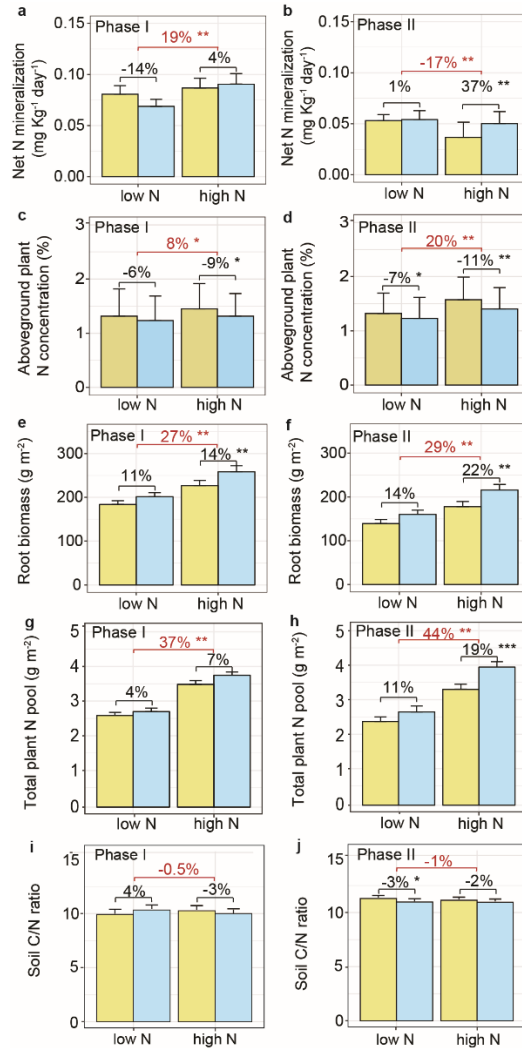
130 **c.4. Estimation of elevated-CO<sub>2</sub> and/or enriched-N induced soil  $R_h$ .** To examine extra  
131 soil heterotrophic respiration ( $R_h$ ) caused by eCO<sub>2</sub> and/or eN, percent changes of simulated

132  $R_h$  in response to eCO<sub>2</sub> and/or eN treatment ( $\% \Delta R_{h,treatment}$ ) was calculated based on Eq.  
 133 7. As a preliminary test of global significance, we extrapolated our results to the world's  
 134 grasslands (19): the annual soil CO<sub>2</sub> efflux ( $R_s$ ) was 8.0 Pg C yr<sup>-1</sup> in the global grasslands,  
 135 which meant  $R_{h,global} = 4.2$  Pg C yr<sup>-1</sup> in global grasslands based on the relationship between  
 136  $R_h$  and  $R_s$  reported by Bond-Lamberty & Thomson (20). We then estimate eCO<sub>2</sub> and/or eN  
 137 would result in more soil C loss as additional  $R_h$  ( $\Delta R_{h,global}$ ):

$$138 \quad \Delta R_{h,global} = R_{h,global} \times \% \Delta R_{h,treatment} = R_{h,global} \times \frac{R_{h,treatment} - R_{h,aCO_2-aN}}{R_{h,aCO_2-aN}} \quad (7)$$

139 where  $R_{h,global}$  (Pg C yr<sup>-1</sup>) is annual  $R_h$  from global grasslands;  $\Delta R_{h,global}$  is the extra  $R_h$   
 140 (Pg C yr<sup>-1</sup>) from global grasslands;  $R_{h,aCO_2-aN}$  denotes the mean annual  $R_h$  (g C m<sup>-2</sup> yr<sup>-1</sup>)  
 141 at aCO<sub>2</sub>-aN, and  $R_{h,treatment}$  is the mean annual  $R_h$  (g C m<sup>-2</sup> yr<sup>-1</sup>) under a specific  
 142 treatment, i.e., eCO<sub>2</sub>-aN, aCO<sub>2</sub>-eN, or eCO<sub>2</sub>-eN.

143

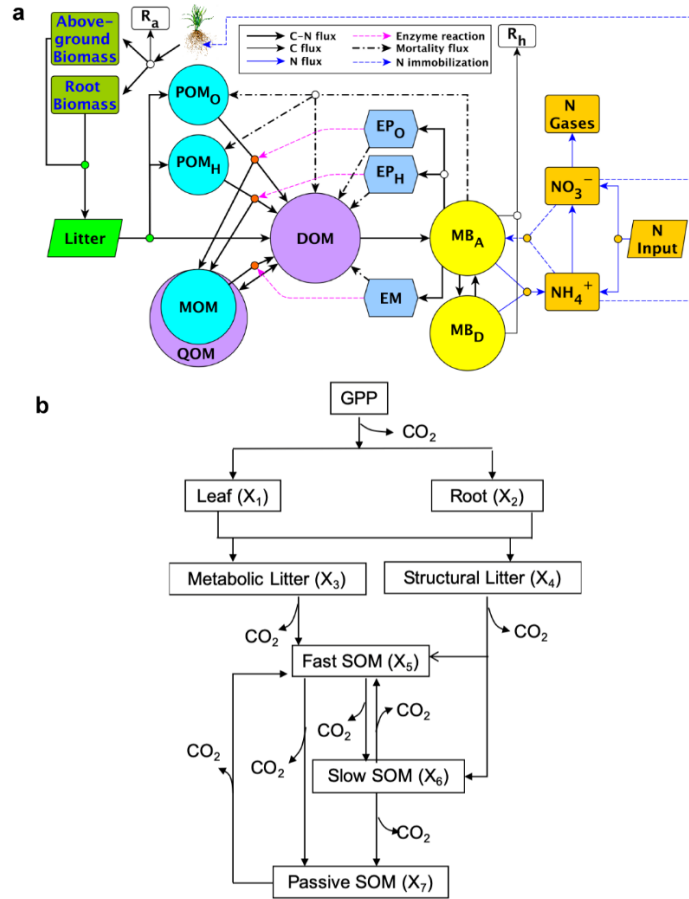


144

145 **Figure S1. The elevated CO<sub>2</sub> (eCO<sub>2</sub>) and enriched N (eN) effects on soil and plant**  
 146 **variables.** Yellow bars represent aCO<sub>2</sub> plots and blue bars represent eCO<sub>2</sub> plots. The  
 147 eCO<sub>2</sub> and the eN effect in Phase I (1998-2005) and Phase II (2006-2009) are shown.  
 148 Percent changes of means of the variables in eCO<sub>2</sub> plots relative to aCO<sub>2</sub> plots at low and  
 149 high N supply, respectively, are labeled in black above the bars. Percent changes in the  
 150 means of all eN plots relative to all aN plots are labeled in red above the bars. **a-b**, soil  
 151 net N mineralization rate (mg kg<sup>-1</sup> day<sup>-1</sup>, averaged for one mid-growing season period per  
 152 year). **c-d**, aboveground plant N concentration (% , measured once in August per year). **e-**  
 153 **f**, root biomass (g/m<sup>2</sup>, 0-20 cm depth measured twice per year). **g-h**, total plant N pool (g  
 154 N m<sup>-2</sup>, measured once in August per year). **i-j**, soil C/N ratio (measured once in 2002 and  
 155 2007, respectively). *p* values of the permutation *t*-test are labeled as \*\*\* when *p* < 0.01,  
 156 \*\* when *p* < 0.01 and \* when *p* < 0.10.

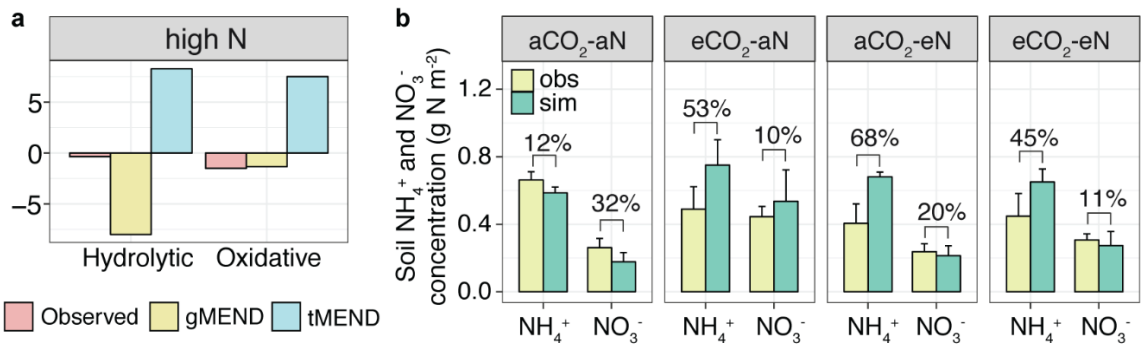
157





158

159 **Figure S2. Structure of ecosystem models.** **a**, Carbon-Nitrogen coupled Microbial-  
 160 ENzyme Decomposition (MEND) model.  $R_a$  and  $R_h$  are autotrophic and heterotrophic  
 161 respiration, respectively.  $POM_O$  and  $POM_H$  are particulate organic matter (POM)  
 162 decomposed by oxidative ( $EP_O$ ) and hydrolytic enzymes ( $EP_H$ ), respectively. MOM is  
 163 mineral-associated OM, which is decomposed by a mixed enzyme group EM. Dissolved  
 164 OM (DOM) interacts with the active layer of MOM (QOM) through sorption and  
 165 desorption. Litter enters  $POM_O$ ,  $POM_H$ , and DOM. Microbes consist of active ( $MB_A$ ) and  
 166 dormant ( $MB_D$ ) microbes. DOM can be assimilated by  $MB_A$ . Ammonium ( $NH_4^+$ ) and  
 167 nitrate ( $NO_3^-$ ) can be immobilized by microbes and taken up by plants. **b**, Terrestrial  
 168 Ecosystem (TECO) model.



169

170 **Figure S3. a**, Comparison of eCO<sub>2</sub> induced percent changes of hydrolytic and oxidative  
 171 enzymes observed by GeoChip to the simulated effects by gMEND (gene-incorporated  
 172 MEND model) and traditional MEND without gene information (tMEND) at high N  
 173 supply. **b**, Comparison of gMEND-simulated (sim) versus observed (obs) mean soil  
 174 ammonium (NH<sub>4</sub><sup>+</sup>) and nitrate (NO<sub>3</sub><sup>-</sup>) concentrations across 12 experimental years. The  
 175 percentages represent the absolute values of percent bias ( $|PBIAS|$ ) between simulated and  
 176 observed mean concentrations.  $|PBIAS| < 70\%$  is generally considered as satisfactory for  
 177 N simulations (21).

178

179 **Table S1.** Trend tests for detecting the changing point of CO<sub>2</sub>×N interactive effects on  
 180 soil CO<sub>2</sub> efflux.

181

Trend test	Change month (n = 47)	<i>p</i>	Change year (n = 12)	<i>p</i>
Pettitt's test	June-2005	0.0005	2005	0.0490
Buishand range test	June-2005	0.0030	2005	0.1037
Buishand U test	June-2005	0.0021	2005	0.0290
Standard Normal Homogeneity Test (SNHT)	July-2005	0.0014	2005	0.0338

182 **Table S2.** Summary of the three-way interactive effects of CO<sub>2</sub>, N, and phase on soil and  
 183 plant variables based on repeated-measures mixed model across 296 plots. Significant (*p*  
 184 < 0.05) effects are bolded.

185

Category	Variables	CO <sub>2</sub> ×N×Phase <sup>[1]</sup>	
		F	<i>p</i>
Soil processes and variables	Soil CO <sub>2</sub> flux	5.260	<b>0.022</b>
	Soil net N mineralization	33.587	<b>&lt;0.001</b>
	Soil temperature	0.039	0.843
	Soil moisture	0.012	0.913
	Soil pH	0.593	0.441
Aboveground plant variables	Aboveground plant N concentration	13.778	<b>&lt; 0.001</b>
	Aboveground plant C/N ratio	0.119	0.730
	Aboveground plant N pool <sup>[2]</sup>	0.018	0.894
	Aboveground plant biomass	0.075	0.785
Root variables	Root N concentration	0.890	0.345
	Root C/N ratio	1.527	0.217
	Root N pool <sup>[2]</sup>	0.453	0.501
	Root biomass	0.354	0.552

186 <sup>[1]</sup> Two levels of Phase: Phase I (1998-2005) and Phase II (2006-2009)

187 <sup>[2]</sup> The N pool was calculated as plant biomass × plant N concentration (%)

188

189 **Table S3.** Main and interactive effects of CO<sub>2</sub>, N, and plant diversity (PD) on soil CO<sub>2</sub>  
 190 efflux in Phase I and Phase II based on repeated-measures mixed model across 296 plots.  
 191 Significant ( $p < 0.05$ ) effects are bolded.

	Phase I		Phase II	
	(1998-2005)		(2006-2009)	
	F	<i>p</i>	F	<i>p</i>
CO <sub>2</sub>	147.61	<b>&lt;0.01</b>	48.27	<b>&lt;0.01</b>
N	12.01	<b>&lt;0.01</b>	14.02	<b>&lt;0.01</b>
PD	104.80	<b>&lt;0.01</b>	13.96	<b>&lt;0.01</b>
CO <sub>2</sub> ×N	3.35	0.07	26.90	<b>&lt;0.01</b>
CO <sub>2</sub> ×PD	0.11	0.74	3.76	<b>0.05</b>
N×PD	0.17	0.68	0.34	0.56
CO <sub>2</sub> ×N×PD	2.26	0.13	2.32	0.13

192

193 **Table S4.** Pearson correlation between CO<sub>2</sub>×N effect (N influence on eCO<sub>2</sub> effect<sup>[1]</sup>) on  
 194 soil CO<sub>2</sub> efflux and CO<sub>2</sub>×N effects on soil/plant variables from 1998 to 2009.

Category	Variables	<i>r</i> <sup>[2]</sup>	<i>p</i> <sup>[2]</sup>
Soil processes	Soil net N mineralization	0.595	<b>0.048</b>
	Soil temperature	0.001	0.998
	Soil moisture	-0.353	0.260
	Soil pH	-0.567	0.055
Aboveground plant variables	Aboveground plant N concentration	0.607	<b>0.037</b>
	Aboveground plant C/N ratio	-0.619	<b>0.032</b>
	Aboveground plant N pool	0.458	0.134
	Aboveground plant biomass	-0.038	0.907
Root variables	Root N concentration	-0.233	0.467
	Root C/N ratio	-0.003	0.993
	Root N pool	0.073	0.822
	Root biomass	0.176	0.584

195 <sup>[1]</sup> eCO<sub>2</sub> effect: calculated by response ratio (RR); N influence on eCO<sub>2</sub> effect: RR at high  
 196 N supply – RR at low N supply

197 <sup>[2]</sup> *r*: correlation coefficient; *p*: significance of the correlation.

198

199 **Table S5.** eCO<sub>2</sub> effects on soil temperature, moisture, and root N concentration at low  
200 and high N supply.

N treatment	CO <sub>2</sub> treatment	Soil temperature	Soil moisture	Root N concentration
Low N	eCO <sub>2</sub> v.s aCO <sub>2</sub>	0.562 <sup>[1]</sup>	0.773	0.981
High N	eCO <sub>2</sub> v.s aCO <sub>2</sub>	0.248	0.564	0.248

201 <sup>[1]</sup>*p* values of the Wilcox test

202

203 **Table S6.** Main and interactive effects of CO<sub>2</sub>, N, and plant diversity (PD) on overall  
 204 relative abundance of microbial functional genes based on permutational multivariate  
 205 analysis of variance (Adonis) across 296 plots.

	Overall abundance of microbial functional genes <sup>[1]</sup>	
	<i>F</i>	<i>p</i>
CO <sub>2</sub>	1.82	<b>0.01</b>
N	1.61	<b>0.03</b>
PD	2.39	<b>&lt;0.01</b>
CO <sub>2</sub> ×N	1.38	<b>0.04</b>
CO <sub>2</sub> ×PD	1.38	0.06
N×PD	1.15	0.18
CO <sub>2</sub> ×N×PD	1.05	0.28
Whole model R <sup>2</sup>	0.04	<b>0.04</b>

206 <sup>[1]</sup> Abundance of microbial functional genes was the normalized signal intensity based on  
 207 GeoChip hybridization. The GeoChip arrays contained a variety of functional genes  
 208 involved in biogeochemical cycling processes (22). PD stands for plant diversity.  
 209 Significant ( $p < 0.05$ ) effects are bolded.



210 **Table S7.** Correlations between the relative abundance of different microbial gene  
 211 categories and soil CO<sub>2</sub> efflux by Mantel test. The relative abundances of microbial genes  
 212 in different gene categories were measured in 2009. Soil CO<sub>2</sub> efflux was averaged in Phase  
 213 I (1998-2005) or Phase II (2006-2009) per plot for the correlation analysis.

Gene category	Phase I		Phase II	
	<i>r</i>	<i>p</i>	<i>r</i>	<i>p</i>
Starch	-0.025	0.798	0.043	0.097
Hemicellulose	-0.040	0.909	0.041	0.100
Cellulose	-0.038	0.894	0.069	0.016
Chitin	-0.040	0.873	0.055	0.057
Pectin	-0.017	0.691	0.041	0.096
Lignin	-0.028	0.780	0.063	0.028
Assimilatory N reduction	-0.035	0.855	0.060	0.036
Dissimilatory N reduction	-0.040	0.887	0.047	0.073
Denitrification	-0.033	0.834	0.048	0.074
Ammonification	-0.023	0.746	0.050	0.048
Nitrification	-0.031	0.853	0.047	0.061
N fixation	-0.041	0.895	0.049	0.074

214

215 **Table S8.** Interactive effects of CO<sub>2</sub> and N on C degradation and N cycling genes.

Gene category	Gene name	eCO <sub>2</sub> effect at aN <sup>[1]</sup> (%)	eCO <sub>2</sub> effect at eN <sup>[2]</sup> (%)	eN effect <sup>[3]</sup> (%)	OE <sup>[4]</sup> (%)	EE <sup>[5]</sup> (%)	OE-EE (%)	CO <sub>2</sub> ×N interaction <sup>[6]</sup>	Adonis p <sup>[7]</sup>
Starch	<i>amyA</i>	4.6	-1.71	1.62	2.56	6.22	-3.66	<b>antagonistic</b>	<b>0.048</b>
	<i>amyX</i>	10.26	12.26	16.47	21.49	26.73	-5.24	additive	0.154
	<i>glucoamylase</i>	9.88	-2.69	6.27	6.24	16.15	-9.91	<b>antagonistic</b>	<b>0.006</b>
	<i>pulA</i>	6.22	-1.84	3.43	3.91	9.65	-5.74	<b>antagonistic</b>	<b>0.008</b>
	<i>isopullulanase</i>	33.42	-6.53	17.72	14.55	51.14	-36.59	<b>antagonistic</b>	<b>0.002</b>
	<i>nplT</i>	3.32	0.43	3.74	3.18	7.06	-3.87	additive	0.246
	<i>apu</i>	15.76	5.38	8.02	11.46	23.78	-12.33	additive	0.462
Hemicel- lulose	<i>ara</i>	4.42	-2.67	1.06	1.33	5.48	-4.15	additive	0.085
	<i>ara_fungi</i>	5.58	-0.70	4.01	3.94	9.59	-5.65	additive	0.324
	<i>xylA</i>	6.19	-2.12	3.18	3.32	9.37	-6.05	<b>antagonistic</b>	<b>0.046</b>
	<i>xylanase</i>	5.69	-1.18	2.45	3.37	8.14	-4.76	additive	0.150
Cellulose	<i>CDH</i>	4.35	-2.34	1.86	1.75	6.21	-4.45	<b>antagonistic</b>	<b>0.028</b>
	<i>cellobiase</i>	5.82	-0.85	5.00	4.5	10.82	-6.32	<b>antagonistic</b>	<b>0.014</b>
	<i>endoglucanase</i>	4.28	-1.17	2.01	2.66	6.29	-3.62	<b>antagonistic</b>	<b>0.032</b>
	<i>exoglucanase</i>	8.21	0.26	8.52	6.57	16.73	-10.16	<b>antagonistic</b>	<b>0.020</b>
Chitin	<i>acetyl-glucosaminidase</i>	4.15	-1.99	1.31	1.79	5.46	-3.68	additive	0.216
	<i>endochitinase</i>	5.42	-1.68	2.37	3.31	7.79	-4.48	<b>antagonistic</b>	<b>0.040</b>
	<i>exochitinase</i>	4.81	1.79	6.01	5.68	10.82	-5.14	<b>antagonistic</b>	<b>0.048</b>
Pectin	<i>pectinase</i>	9.01	0.55	6.14	8.02	15.15	-7.13	<b>antagonistic</b>	<b>0.011</b>
Aromatic s	<i>limEH</i>	5.08	-0.88	2.44	3.28	7.52	-4.24	additive	0.190
	<i>vanA</i>	3.47	-1.52	1.18	1.62	4.65	-3.03	additive	0.173
	<i>vdh</i>	5.35	-1.86	2.31	2.47	7.66	-5.2	additive	0.153
Lignin	<i>glx</i>	4.94	-1.17	2.73	3.45	7.67	-4.23	<b>antagonistic</b>	<b>0.014</b>
	<i>lip</i>	6.6	-0.94	3.97	5.04	10.57	-5.53	<b>antagonistic</b>	<b>0.036</b>
	<i>mnp</i>	10.8	-2.42	5.36	6.85	16.16	-9.3	<b>antagonistic</b>	<b>0.036</b>
	<i>phenol_oxidase</i>	6.75	-1.29	3.59	4.74	10.34	-5.6	<b>antagonistic</b>	<b>0.036</b>
	<i>camDCAB</i>	7.41	-1.83	7.36	1.63	14.77	-13.13	<b>antagonistic</b>	<b>0.016</b>
N reductio- n	<i>napA</i>	6.11	-0.79	3.15	4.36	9.26	-4.9	additive	0.234
	<i>nrfA</i>	3.83	-2.08	1.03	1.16	4.86	-3.7	<b>antagonistic</b>	<b>0.042</b>
	<i>nasA</i>	7.94	-2.21	3.72	4.51	11.66	-7.15	<b>antagonistic</b>	<b>0.020</b>
Denitrifi- cation	<i>narG</i>	4.25	-2.07	1.42	1.71	5.67	-3.95	additive	0.114
	<i>nirK</i>	5.76	-2.19	2.43	2.94	8.19	-5.25	additive	0.138
	<i>nirS</i>	9.3	-2.79	4.19	5.15	13.49	-8.34	<b>antagonistic</b>	<b>0.019</b>
	<i>norB</i>	3.82	-0.15	3.16	2.91	6.98	-4.08	additive	0.090
	<i>nosZ</i>	8.87	-1.81	5.19	5.87	14.06	-8.19	<b>antagonistic</b>	<b>0.031</b>

Ammonification	<i>gdh</i>	10.2	-2.64	5.97	6.09	16.17	-10.09	<b>antagonistic</b>	<b>0.004</b>
	<i>ureC</i>	4.02	-1.86	2.63	1.85	6.65	-4.8	<b>antagonistic</b>	<b>0.038</b>
Nitrification	<i>amoA</i>	4.72	-0.96	2.97	3.23	7.69	-4.45	<b>antagonistic</b>	<b>0.016</b>
	<i>nifH</i>	7.15	-0.74	4.92	5.64	12.07	-6.42	<b>antagonistic</b>	<b>0.046</b>

216 <sup>[1]</sup> eCO<sub>2</sub> effect at aN (%): calculated as  $100\% \times \frac{\overline{eCaN} - \overline{aCaN}}{\overline{aCaN}}$ , where  $\overline{eCaN}$  and  $\overline{aCaN}$   
217 represent the mean of gene abundance in elevated CO<sub>2</sub>-low N and ambient CO<sub>2</sub>-low N  
218 plots, respectively.

219 <sup>[2]</sup> eCO<sub>2</sub> effect at eN (%): calculated as  $100\% \times \frac{\overline{eCeN} - \overline{aCeN}}{\overline{aCeN}}$ , where  $\overline{eCeN}$  and  $\overline{aCeN}$   
220 represent the mean of gene abundance in elevated CO<sub>2</sub>-high N and ambient CO<sub>2</sub>-high N  
221 plots, respectively.

222 <sup>[3]</sup> eN effect (%): calculated as  $100\% \times \frac{\overline{aCeN} - \overline{aCaN}}{\overline{aCaN}}$ , where  $\overline{aCeN}$  represent the mean of  
223 gene abundance in ambient CO<sub>2</sub>-high N plots.

224 <sup>[4]</sup> Observed Effect (OE): calculated as  $100\% \times \frac{\overline{eCeN} - \overline{aCaN}}{\overline{aCaN}}$ , where  $\overline{eCeN}$  represent the  
225 mean of gene abundance in elevated CO<sub>2</sub>-high N plots.

226 <sup>[5]</sup> Expected Effect (EE): calculated as  $100\% \times \frac{\overline{eCaN} - \overline{aCaN}}{\overline{aCaN}} + 100\% \times \frac{\overline{aCeN} - \overline{aCaN}}{\overline{aCaN}}$ .

227 <sup>[6]</sup> Interactive effect is additive when EE does not differ from OE, synergistic when EE is  
228 significantly smaller than OE, or antagonistic when EE is significantly larger than OE.

229 <sup>[7]</sup> The significance of the CO<sub>2</sub>×N effect on the abundance matrix of each gene was tested  
230 by permutational multivariate analysis of variance (Adonis). Significant ( $p < 0.05$ ) effects  
231 are bolded.

232

233 **Table S9.** Interactive effects of CO<sub>2</sub> and N on bacterial and fungal genes related to C  
 234 degradation and N cycling.

Kingdom	Gene name	eCO <sub>2</sub> effect at aN <sup>[1]</sup> (%)	eCO <sub>2</sub> effect at eN <sup>[2]</sup> (%)	eN effect <sup>[3]</sup> (%)	OE <sup>[4]</sup> (%)	EE <sup>[5]</sup> (%)	OE-EE (%)	CO <sub>2</sub> ×N interaction <sup>[6]</sup>	Adonis <i>p</i> <sup>[7]</sup>
Bacteria	<i>amyA</i>	1.64	-1.72	4.52	2.49	6.17	-3.67	<b>antagonistic</b>	<b>0.05</b>
	<i>glucoamylase</i>	5.61	-3.81	11.24	6.20	16.8	-10.6	<b>antagonistic</b>	<b>0.04</b>
	<i>xylA</i>	3.06	-2.14	6.11	3.21	9.17	-5.96	<b>antagonistic</b>	<b>0.05</b>
	<i>CDH</i>	1.85	-2.34	4.34	1.74	6.20	-4.45	<b>antagonistic</b>	<b>0.04</b>
	<i>exochitinase</i>	5.72	2.17	3.81	5.05	9.54	-4.48	<b>antagonistic</b>	<b>0.05</b>
	<i>nrjA</i>	1.03	-2.08	3.82	1.15	4.85	-3.70	<b>antagonistic</b>	<b>0.03</b>
	<i>nirS</i>	4.32	-2.90	9.36	5.05	13.68	-8.63	<b>antagonistic</b>	<b>0.01</b>
	<i>nosZ</i>	5.12	-1.94	8.89	5.74	14.01	-8.26	<b>antagonistic</b>	<b>0.03</b>
	<i>gdh</i>	5.99	-3.24	10.84	6.29	16.84	-10.54	<b>antagonistic</b>	<b>0.01</b>
	<i>ureC</i>	2.67	-2.08	4.16	1.75	6.83	-5.08	<b>antagonistic</b>	<b>0.02</b>
Fungi	<i>amoA</i>	2.24	-1.27	4.22	2.47	6.46	-3.98	<b>antagonistic</b>	<b>0.05</b>
	<i>glucoamylase</i>	18.90	0.63	16.72	15.65	35.62	-19.97	<b>antagonistic</b>	<b>0.03</b>
	<i>endoglucanase</i>	4.30	0.73	5.80	5.52	10.10	-4.58	<b>antagonistic</b>	<b>0.04</b>
	<i>pectinase</i>	6.50	0.72	7.22	6.18	13.73	-7.54	<b>antagonistic</b>	<b>0.01</b>

235 <sup>[1], [2], [3], [4], [5], [6], [7]</sup> The parameters are described in Table S8.

236 Only genes that are significantly ( $p < 0.05$ ) affected by CO<sub>2</sub>×N are shown.

237

238 **Table S10.** Predictions of significant changes between eCO<sub>2</sub> and aCO<sub>2</sub> at low or high N  
 239 supply based on the two competing theories: stoichiometric decomposition and microbial  
 240 N mining. The following predictions are based on literature analyses and synthesis. Since  
 241 the interactive effects between CO<sub>2</sub> and N on the responses of ecosystems are very  
 242 complicated, the following listed predictions could vary considerably among different  
 243 ecosystems. For the purpose of this study, we attempt to just list the possible CO<sub>2</sub>×N effects  
 244 based on data available from BioCON experimental sites. Those effects are not necessarily  
 245 applicable to other ecosystems. +, significantly stimulation; -, Significantly repress; 0, no  
 246 significant changes.

Properties	Stoichiometric decomposition		Microbial N mining	
	low N	high N	low N	high N
Soil CO <sub>2</sub> efflux	- <sup>[1]</sup> or + <sup>[2]</sup>	+ <sup>[3]</sup>	+ <sup>[6]</sup>	- <sup>[7]</sup>
Labile C genes	- <sup>[1]</sup>	+ <sup>[4]</sup>	+ <sup>[6]</sup>	+ <sup>[8]</sup>
Recalcitrant C genes	- <sup>[1]</sup>	+ <sup>[5]</sup>	+ <sup>[6]</sup>	- <sup>[7]</sup>
N genes	- <sup>[1]</sup>	+ <sup>[5]</sup>	+ <sup>[5]</sup>	- <sup>[7]</sup>
Interactive effects	Synergistic	Synergistic	Antagonistic	Antagonistic

247 <sup>[1]</sup> eCO<sub>2</sub> generally increases the C/N ratios of plant tissues, leading to higher litter and soil  
 248 C/N ratios (23, 24). Higher substrate C/N ratio may, in turn, result in nutrient limitation,  
 249 which inhibits microbial growth and reduces microbial activity like C decomposition and  
 250 respiration rate (25-28).

251 <sup>[2]</sup> Low N availability will not inhibit the microbial uptake of both substrate C and other  
 252 nutrients, but excessive C is routed to overflow respiration (29, 30).

253 <sup>[3]</sup> Plant N content relative to C is one to two orders of magnitude lower than microbial  
 254 biomass (31). Because of this different stoichiometry and considering that eCO<sub>2</sub> generally  
 255 increases plant C and N ratios (23, 24), microbes degrade plant litter with an initial higher  
 256 N concentration more quickly.

257 <sup>[4]</sup> Due to the larger contribution of rapid-growing microbes (r-strategists) utilizing eCO<sub>2</sub>  
 258 stimulated labile C inputs (32).

259 <sup>[5]</sup> Due to co-metabolism of soil C and other nutrients (33).

260 <sup>[6]</sup> eCO<sub>2</sub> generally increases labile C inputs into soils (34), resulting in a larger contribution  
 261 of slow-growing microbes (K-strategists) to utilize labile C as the energy source to  
 262 decompose recalcitrant C for N acquirement (32, 35).

263 <sup>[7]</sup> Due to suppressed microbial mining of recalcitrant C for N in soils with high N  
264 availability (25, 36).

265 <sup>[8]</sup> High N availability increases the rate of labile C utilization by microbes for growth  
266 (increase in microbial assimilation rates) (25, 37).

267 **Table S11.** Objective functions used for different response variables in the MEND  
 268 model parameterization.

Response Variable	Description	Objective Function
$R_s$ (CO <sub>2</sub> )	Soil CO <sub>2</sub> efflux = root respiration ( $R_a$ ) + microbial respiration ( $R_h$ )	<sup>[1]</sup> $R^2$ between Simulated $R_s$ and Observed $R_s$
NH <sub>4</sub> <sup>+</sup>	Ammonium concentration	<sup>[2]</sup> $PBIAS$ between Simulated and Observed NH <sub>4</sub> <sup>+</sup>
NO <sub>3</sub> <sup>-</sup>	Nitrate concentration	$PBIAS$ between Simulated and Observed NO <sub>3</sub> <sup>-</sup>
EnzCo	Concentration (EnzC) of Oxidative Enzyme	$MARE$ <sup>[3]</sup> between Simulated EnzC and Expected EnzC Expected EnzC = Simulated EnzC at ambient N × RR <sup>[4]</sup>
EnzCh	Hydrolytic Enzyme Concentration	$MARE$ between Simulated EnzC and Expected EnzC Expected EnzC = Simulated EnzC at ambient N × RR

269 <sup>[1]</sup>  $R^2$  denotes the coefficient of determination, see Method Eq. 4.

270 <sup>[2]</sup>  $PBIAS$  is the percent bias between observations and simulations, , see Method Eq. 6.

271 <sup>[3]</sup>  $MARE$  is the mean absolute relative error, see Methods Eq. 5.

272 <sup>[4]</sup> RR is the ratio of gene abundance at eCO<sub>2</sub>-aN or eCO<sub>2</sub>-eN to that at aCO<sub>2</sub>-aN or aCO<sub>2</sub>-  
 273 eN, i.e.,  $RR_{aN} = eCO_2\text{-aN}/aCO_2\text{-aN}$ ,  $RR_{eN} = eCO_2\text{-eN}/aCO_2\text{-eN}$ .

274

275 **Table S12.** Soil C and N pools (state variables) in the MEND model.

ID	Soil C and/or N pool	Pool Name	Variable name in equations
1	Particulate organic matter (POM) decomposed by oxidative enzymes	POM <sub>O</sub>	C pool: $P_O$ ; N pool: $PN_O$
2	POM decomposed by hydrolytic enzymes	POM <sub>H</sub>	$P_H$ ; $PN_H$
3	Mineral-associated organic matter	MOM	$M$ ; $MN$
4	Dissolved organic matter	DOM	$D$ ; $DN$
5	Active MOM interacting with DOM	QOM	$Q$ ; $QN$
6	Active microbial biomass	MB <sub>A</sub>	$BA$ ; $BAN$
7	Dormant microbial biomass	MB <sub>D</sub>	$BD$ ; $BDN$
8	Oxidative enzymes decomposing POM <sub>O</sub>	EP <sub>O</sub>	$EP_O$ ; $EPN_O$
9	Hydrolytic enzymes decomposing POM <sub>H</sub>	EP <sub>H</sub>	$EP_H$ ; $EPN_H$
10	Enzymes decomposing MOM	EM	$EM$ ; $EMN$
11	Ammonium	NH <sub>4</sub> <sup>+</sup>	$NH_4$
12	Nitrate	NO <sub>3</sub> <sup>-</sup>	$NO_3$

276



**Table S13.** Governing equation for each soil C or N pool in the MEND model<sup>a</sup>.

Governing Equation	Eq#
<b>Soil C (state variable, e.g., <math>P_1</math>, denotes the C content):</b>	
$\frac{dP_O}{dt} = I_{P_O} + (1 - g_D) \cdot g_{P_O} \cdot F_{14} - F_1$	(S1)
$\frac{dP_H}{dt} = I_{P_H} + (1 - g_D) \cdot (1 - g_{P_O}) \cdot F_{14} - F_2$	(S2)
$\frac{dM}{dt} = (1 - f_D) \cdot (F_1 + F_2) - F_3$	(S3)
$\frac{dQ}{dt} = F_4 - F_5$	(S4)
$\frac{dD}{dt} = I_D + f_D \cdot (F_1 + F_2) + F_3 + g_D \cdot F_{14} + F_{16} - F_6 - (F_4 - F_5)$	(S5)
$\frac{dBA}{dt} = F_6 - (F_7 - F_8) - (F_9 + F_{10} + F_{11}) - F_{14} - F_{15}$	(S6)
$\frac{dBD}{dt} = (F_7 - F_8) - (F_{12} + F_{13})$	(S7)
$\frac{dEP_O}{dt} = F_{15,EPO} - F_{16,EPO}$	(S8)
$\frac{dEP_H}{dt} = F_{15,EPH} - F_{16,EPH}$	(S9)
$\frac{dEM}{dt} = F_{15,EM} - F_{16,EM}$	(S10)
$\frac{dCO_2}{dt} = R_h = (F_9 + F_{10} + F_{11}) + (F_{12} + F_{13})$	(S11)
$\frac{d}{dt} (P_O + P_H + M + Q + D + BA + BD + EP_O + EP_H + EM)$ $= (I_{P_O} + I_{P_H} + I_D) - (F_9 + F_{10} + F_{11}) - (F_{12} + F_{13})$	(S12)
<b>Soil N (state variable, e.g., <math>PN_1</math>, denotes the N content):</b>	
For $PN_O$ , $PN_H$ , $MN$ , $QN$ , and $DN$ , the N flux is calculated as: $FN_i = F_i / CN_{source}$ where $F_i$ is the C flux, and $CN_{source}$ is the C:N ratio of the (upstream) source pool	(S13)
$\frac{dBAN}{dt} = \frac{F_6}{CN_D} - \left( \frac{F_7}{CN_{BA}} - \frac{F_8}{CN_{BD}} \right) - \frac{F_{12}}{CN_{BA}} - \frac{F_{13}}{CN_{ENZ}} - FN_{mn,BA}$ $+ (FN_{im,NH_4 \rightarrow BA} + FN_{im,NO_3 \rightarrow BA})$	(S14)
$\frac{dBDN}{dt} = \left( \frac{F_7}{CN_{BA}} - \frac{F_8}{CN_{BD}} \right) - FN_{mn,BD}$	(S15)
$\frac{dNH_4}{dt} = I_{NH_4} + (FN_{mn,BA} + FN_{mn,BD}) - FN_{im,NH_4 \rightarrow BA} - FN_{nit}$	(S16)
$\frac{dNO_3}{dt} = I_{NO_3} + FN_{nit} - FN_{nit-denit} - FN_{denit} - FN_{im,NO_3 \rightarrow BA}$	(S17)
$\frac{d}{dt} (PN_O + PN_H + MN + QN + DN + BAN + BDN + EPN_O + EPN_H + EMN + NH_4 + NO_3)$ $= (IN_{P_O} + IN_{P_H} + IN_D + I_{NH_4} + I_{NO_3}) - (FN_{nit-denit} + FN_{denit})$	(S18)

278 <sup>[1]</sup> The state variables (C and N pools) are described in Table S12; Eq. S11 indicates the  
279 total heterotrophic respiration flux ( $R_h$ ); Eq. S12 and S18 express the overall mass balance  
280 of C and N, respectively. The transformation fluxes ( $F$  or  $FN$ ) are elucidated by Eqs. S19–  
281 S41 in Table S14.

282

283 **Table S14.** Component fluxes in the MEND model (parameters are described in Table  
 284 S10).

Flux description	Equation	Eq#
Particulate organic matter (POM) pool (oxidative) ( $P_O$ ) decomposition ( $F_1$ )	$F_1 = \frac{Vd_{P_O} \cdot EP_O \cdot P_O}{K_{P_O} + P_O}$	(S19)
POM pool (hydrolytic) ( $P_H$ ) decomposition	$F_2 = \frac{Vd_{P_H} \cdot EP_H \cdot P_H}{K_{P_H} + P_H}$	(S20)
Mineral-associated organic matter (MOM, $M$ ) decomposition	$F_3 = \frac{Vd_M \cdot EM \cdot M}{K_M + M}$	(S21)
Adsorption ( $F_4$ ) and desorption ( $F_5$ ) between dissolved organic matter (DOM, $D$ ) and adsorbed DON (QOM, $Q$ )	$F_4 = k_{ads} \cdot (1 - Q/Q_{max}) \cdot D$ $F_5 = k_{des} \cdot (Q/Q_{max})$	(S22) (S23)
DOM ( $D$ ) uptake by microbes	$F_6 = \frac{1}{Y_g} (V_g + V_m) \cdot \frac{BA \cdot D}{K_D + D}$	(S24)
Dormancy ( $F_7$ ) and reactivation ( $F_8$ ) between active ( $MB_A$ , $BA$ ) and dormant ( $MB_D$ , $BD$ ) microbes	$F_7 = [1 - D/(K_D + D)] \cdot V_m \cdot BA$ $F_8 = [D/(K_D + D)] \cdot V_m \cdot BD$	(S25) (S26)
$MB_A$ ( $BA$ ) growth respiration ( $F_9$ ) and maintenance respiration ( $F_{10}$ )	$F_9 = \left(\frac{1}{Y_g} - 1\right) \cdot \frac{V_g \cdot BA \cdot D}{K_D + D}$ $F_{10} = \left(\frac{1}{Y_g} - 1\right) \cdot \frac{V_m \cdot BA \cdot D}{K_D + D}$	(S27) (S28)
$MB_A$ ( $BA$ ) overflow respiration ( $F_{11}$ )	$F_{11} = \max\{0, BA - BAN \cdot CN_{BA,max}\}$	(S29)
$MB_D$ ( $BD$ ) maintenance respiration ( $F_{12}$ )	$F_{12} = \beta \cdot V_m \cdot BD$	(S30)
$MB_D$ ( $BD$ ) overflow respiration ( $F_{13}$ )	$F_{13} = \max\{0, BD - BDN \cdot CN_{BA,max}\}$	(S31)
$MB_A$ ( $BA$ ) mortality	$F_{14} = \gamma \cdot V_m \cdot BA$	(S32)
Synthesis of enzymes for $P_O$ ( $EP_O$ , $F_{15,EPO}$ ), enzymes for $P_H$ ( $EP_H$ , $F_{15,EPH}$ ), and enzymes for $M$ ( $EM$ , $F_{15,EM}$ )	$F_{15,EPO} = P_O/(P_O + P_H) \cdot p_{EP} \cdot V_m \cdot BA$ $F_{15,EPH} = P_H/(P_O + P_H) \cdot p_{EP} \cdot V_m \cdot BA$ $F_{15,EM} = f p_{EM} \cdot p_{EP} \cdot V_m \cdot BA$ $F_{15} = F_{15,EPO} + F_{15,EPH} + F_{15,EM}$	(S33)
Turnover of enzymes ( $EP_O$ , $EP_H$ , $EM$ )	$F_{16,EPO} = r_E \cdot EP_O, F_{16,EPH} = r_E \cdot EP_H$ $F_{16,EM} = r_E \cdot EM$ $F_{16} = F_{16,EPO} + F_{16,EPH} + F_{16,EM}$	(S34)
N immobilization by microbes	$FN_{im,NH_4 \rightarrow BA} = \frac{(VN_{im,NH_4} \cdot YN_g) \cdot BA \cdot NH_4}{KS_{NH_4} \cdot \left(1 + \frac{NH_4}{KS_{NH_4}} + \frac{NO_3}{KS_{NO_3}} + \frac{BA}{KS_{NH_4}}\right)}$ $FN_{im,NO_3 \rightarrow BA} = \frac{(VN_{im,NO_3} \cdot YN_g) \cdot BA \cdot NO_3}{KS_{NO_3} \cdot \left(1 + \frac{NH_4}{KS_{NH_4}} + \frac{NO_3}{KS_{NO_3}} + \frac{BA}{KS_{NO_3}}\right)}$	(S35) (S36)
N mineralization	$FN_{mn,BA} = (1 - YN_g) \cdot FN_6$	(S37)
	$YN_g = \left(\frac{CN_{BA} - CN_{BA,min}}{CN_{BA,max} - CN_{BA,min}}\right)^\omega$	(S38)
Nitrification	$FN_{nit} = VN_{nit} \cdot NH_4$	(S39)
Nitrifier Denitrification	$FN_{nit-denit} = FN_{nitrif} \cdot [1 - f(O_2)]$ $f(O_2) = \frac{(1-WFP)^{4/3}}{0.5^{4/3} + (1-WFP)^{4/3}}$ $WFP \text{ is water-filled porosity}$	(S40a) (S40b)
Denitrification	$FN_{denit} = VN_{denit} \cdot NO_3$	(S41)

285

286 **Table S15.** MEND model parameters.

ID	Parameter	Description	Units	Eq#
1	$LF_0$	Initial fraction of $P_O$ , $LF_0 = P_O/(P_O+P_H)$	—	
2	$r_0$	Initial active fraction of microbes, $r_0 = BA/(BA+BD)$	—	
3	$fINP$	Scaling factor for litter input rate	—	
4	$Vd_{P_O}$	Maximum specific decomposition rate for $P_O$	mg C mg <sup>-1</sup> C h <sup>-1</sup>	S19
5	$Vd_{P_H}$	Maximum specific decomposition rate for $P_H$	mg C mg <sup>-1</sup> C h <sup>-1</sup>	S20
6	$Vd_M$	Maximum specific decomposition rate for $M$	mg C mg <sup>-1</sup> C h <sup>-1</sup>	S21
7	$K_{P_O}$	Half-saturation constant for $P_O$ decomposition	mg C cm <sup>-3</sup> soil	S19
8	$K_{P_H}$	Half-saturation constant for $P_H$ decomposition	mg C cm <sup>-3</sup> soil	S20
9	$K_M$	Half-saturation constant for $M$ decomposition	mg C cm <sup>-3</sup> soil	S21
10	$Q_{max}$	Maximum sorption capacity	mg C cm <sup>-3</sup> soil	S22
11	$K_{ba}$	Binding affinity, Sorption rate $k_{ads} = k_{des} \times K_{ba}$	(mg C cm <sup>-3</sup> soil) <sup>-1</sup>	S22
12	$k_{des}$	Desorption rate	mg C cm <sup>-3</sup> soil h <sup>-1</sup>	S23
13*	$r_E$	Turnover rate of $EP_O$ , $EP_H$ , and $EM$	mg C mg <sup>-1</sup> C h <sup>-1</sup>	S34
14*	$p_{EP}$	$[V_m \times p_{EP}]$ is the production rate of $EP$ ( $EP_O + EP_H$ ), $V_m$ is the specific maintenance rate for $BA$	—	S33
15*	$f_{pEM}$	$f_{pEM} = p_{EM}/p_{EP}$ , $[V_m \times p_{EM}]$ is the production rate of $EM$	—	S33
16*	$f_D$	Fraction of decomposed $P_O$ and $P_H$ allocated to $D$	—	S3
17*	$g_D$	Fraction of dead $BA$ allocated to $D$	—	S1
18*	$V_g$	Maximum specific uptake rate of $D$ for growth	mg C mg <sup>-1</sup> C h <sup>-1</sup>	S24
19*	$\alpha$	$= V_m / (V_g + V_m)$	—	S24
20*	$K_D$	Half-saturation constant for microbial uptake of $D$	mg C cm <sup>-3</sup> soil	S24
21*	$Y_g(T_{ref})$	True growth yield at reference temperature ( $T_{ref}$ )	—	S24
22	$k_{Y_g}$	Slope for $Y_g$ dependence of temperature	1/°C	S24
23*	$Q_{10}$	Q <sub>10</sub> for temperature response function	—	S24
24	$\gamma$	Max microbial mortality rate = $V_m \times \gamma$	—	S32
25	$\beta$	Ratio of dormant maintenance rate to $V_m$	—	S30
26	$\psi_{A2D}$	Soil water potential (SWP) threshold for microbial dormancy; both $\psi_{A2D}$ & $\psi_{D2A} < 0$	-MPa	S49
27	$\tau$	$\psi_{D2A} = \psi_{A2D} \times \tau$ , $\psi_{D2A}$ is the SWP threshold for microbial resuscitation	—	S50
28	$\omega$	Exponential in SWP function for microbial dormancy or resuscitation	—	S50
29	$VN_{im,NH_4}$	Max specific immobilization rate for $NH_4^+$	mg N mg <sup>-1</sup> C h <sup>-1</sup>	S35
30	$VN_{im,NO_3}$	Max specific immobilization rate for $NO_3^-$	mg N mg <sup>-1</sup> C h <sup>-1</sup>	S36
31	$KS_{NH_4}$	Half-saturation constant for $NH_4^+$ immobilization	mg N cm <sup>-3</sup> soil	S35
32	$KS_{NO_3}$	Half-saturation constant for $NO_3^-$ immobilization	mg N cm <sup>-3</sup> soil	S36
33	$VN_{nit}$	Max nitrification rate	h <sup>-1</sup>	S39
34	$VN_{denit}$	Max denitrification rate	h <sup>-1</sup>	S41

287 \*denotes the 10 parameters calibrated for C cycling processes in this study.

288

289 **References**

- 290 1. X. Zhu *et al.*, Underestimates of Grassland Gross Primary Production in MODIS  
291 Standard Products. *Remote Sensing* **10**, 1771 (2018).
- 292 2. K. Fiala, I. Tůma, P. Holub, Interannual variation in root production in grasslands  
293 affected by artificially modified amount of rainfall. *The Scientific World Journal*  
294 **2012**, 1-10 (2012).
- 295 3. R. Waring, J. Landsberg, M. Williams, Net primary production of forests: a  
296 constant fraction of gross primary production? *Tree physiology* **18**, 129-134  
297 (1998).
- 298 4. W. Parton, D. S. Schimel, C. Cole, D. Ojima, Analysis of factors controlling soil  
299 organic matter levels in Great Plains grasslands. *Soil Science Society of America*  
300 *Journal* **51**, 1173-1179 (1987).
- 301 5. Z. Shi *et al.*, Experimental warming altered rates of carbon processes, allocation,  
302 and carbon storage in a tallgrass prairie. *Ecosphere* **6**, 1-16 (2015).
- 303 6. Q. Y. Duan, S. Sorooshian, V. Gupta, Effective and efficient global optimization  
304 for conceptual rainfall-runoff models. *Water Resources Research* **28**, 1015-1031  
305 (1992).
- 306 7. G. Wang, J. Xia, J. Chen, Quantification of effects of climate variations and  
307 human activities on runoff by a monthly water balance model: a case study of the  
308 Chaobai River basin in northern China. *Water resources research* **45**, 1-12  
309 (2009).
- 310 8. G. Wang *et al.*, Microbial dormancy improves development and experimental  
311 validation of ecosystem model. *ISME J.* **9**, 226-237 (2015).
- 312 9. T. Xu, L. White, D. Hui, Y. Luo, Probabilistic inversion of a terrestrial ecosystem  
313 model: Analysis of uncertainty in parameter estimation and model prediction.  
314 *Global Biogeochemical Cycles* **20**, 1-15 (2006).
- 315 10. G. Wang, S. Chen, Evaluation of a soil greenhouse gas emission model based on  
316 Bayesian inference and MCMC: Model uncertainty. *Ecological modelling* **253**,  
317 97-106 (2013).
- 318 11. P. E. Thornton, N. A. Rosenbloom, Ecosystem model spin-up: Estimating steady  
319 state conditions in a coupled terrestrial carbon and nitrogen cycle model.  
320 *Ecological Modelling* **189**, 25-48 (2005).
- 321 12. G. B. Bonan, M. D. Hartman, W. J. Parton, W. R. Wieder, Evaluating litter  
322 decomposition in earth system models with long - term litterbag experiments: an  
323 example using the Community Land Model version 4 (CLM 4). *Global change*  
324 *biology* **19**, 957-974 (2013).
- 325 13. N. Fanin, N. Fromin, S. Barantal, S. Hättenschwiler, Stoichiometric plasticity of  
326 microbial communities is similar between litter and soil in a tropical rainforest.  
327 *Scientific reports* **7**, 12498 (2017).
- 328 14. G. Wang, W. Huang, G. Zhou, M. A. Mayes, J. Zhou, Modeling the processes of  
329 soil moisture in regulating microbial and carbon-nitrogen cycling. *Journal of*  
330 *Hydrology* **585**, 124777 (2020).
- 331 15. G. Wang, S. Chen, A review on parameterization and uncertainty in modeling  
332 greenhouse gas emissions from soil. *Geoderma* **170**, 206-216 (2012).

- 333 16. J. L. Devore, *Probability and Statistics for Engineering and the Sciences (7th Ed.)*  
334 (Brooks/Cole Cengage Learning, Florence, KY, 2008), pp. 768.
- 335 17. C. W. Dawson, R. J. Abrahart, L. M. See, HydroTest: a web-based toolbox of  
336 evaluation metrics for the standardised assessment of hydrological forecasts.  
337 *Environmental Modelling & Software* **22**, 1034-1052 (2007).
- 338 18. G. Wang, H. I. Jager, L. M. Baskaran, C. C. Brandt, Hydrologic and water quality  
339 responses to biomass production in the Tennessee river basin. *GCB Bioenergy* **10**,  
340 877-893 (2018).
- 341 19. M. Adachi, A. Ito, S. Yonemura, W. Takeuchi, Estimation of global soil  
342 respiration by accounting for land-use changes derived from remote sensing data.  
343 *Journal of environmental management* **200**, 97-104 (2017).
- 344 20. B. Bond-Lamberty, A. Thomson, A global database of soil respiration data.  
345 *Biogeosciences* **7**, 1915-1926 (2010).
- 346 21. D. N. Moriasi *et al.*, Model evaluation guidelines for systematic quantification of  
347 accuracy in watershed simulations. *Transactions of the ASABE* **50**, 885-900  
348 (2007).
- 349 22. Z. He *et al.*, Metagenomic analysis reveals a marked divergence in the structure of  
350 belowground microbial communities at elevated CO<sub>2</sub>. *Ecology Letters* **13**, 564-  
351 575 (2010).
- 352 23. Y. Yang, Y. Luo, M. Lu, C. Schädel, W. Han, Terrestrial C:N stoichiometry in  
353 response to elevated CO<sub>2</sub> and N addition: a synthesis of two meta-analyses. *Plant*  
354 *and Soil* **343**, 393-400 (2011).
- 355 24. R. J. Norby, M. F. Cotrufo, P. Ineson, E. G. O'Neill, J. G. Canadell, Elevated  
356 CO<sub>2</sub>, litter chemistry, and decomposition: a synthesis. *Oecologia* **127**, 153-165  
357 (2001).
- 358 25. J. M. Craine, C. Morrow, N. Fierer, Microbial nitrogen limitation increases  
359 decomposition. *Ecology* **88**, 2105-2113 (2007).
- 360 26. S. Manzoni, J. A. Trofymow, R. B. Jackson, A. Porporato, Stoichiometric controls  
361 on carbon, nitrogen, and phosphorus dynamics in decomposing litter. *Ecological*  
362 *Monographs* **80**, 89-106 (2010).
- 363 27. R. L. Sinsabaugh *et al.*, Stoichiometry of soil enzyme activity at global scale.  
364 *Ecology Letters* **11**, 1252-1264 (2008).
- 365 28. S. Recous, D. Robin, D. Darwis, B. Mary, Soil inorganic N availability: Effect on  
366 maize residue decomposition. *Soil Biology and Biochemistry* **27**, 1529-1538  
367 (1995).
- 368 29. S. Manzoni, A. Porporato, Soil carbon and nitrogen mineralization: theory and  
369 models across scales. *Soil Biology and Biochemistry* **41**, 1355-1379 (2009).
- 370 30. S. Manzoni, P. Taylor, A. Richter, A. Porporato, G. I. Ågren, Environmental and  
371 stoichiometric controls on microbial carbon-use efficiency in soils. *New*  
372 *Phytologist* **196**, 79-91 (2012).
- 373 31. S. Manzoni, R. B. Jackson, J. A. Trofymow, A. Porporato, The global  
374 stoichiometry of litter nitrogen mineralization. *Science* **321**, 684-686 (2008).
- 375 32. E. Blagodatskaya, Y. Kuzyakov, Mechanisms of real and apparent priming effects  
376 and their dependence on soil microbial biomass and community structure: critical  
377 review. *Biology and Fertility of Soils* **45**, 115-131 (2008).

- 378 33. Y. Fang, L. Nazaries, B. K. Singh, B. P. Singh, Microbial mechanisms of carbon  
379 priming effects revealed during the interaction of crop residue and nutrient inputs  
380 in contrasting soils. *Global Change Biology* **24**, 2775-2790 (2018).
- 381 34. R. P. Phillips, A. C. Finzi, E. S. Bernhardt, Enhanced root exudation induces  
382 microbial feedbacks to N cycling in a pine forest under long-term CO<sub>2</sub>  
383 fumigation. *Ecology Letters* **14**, 187-194 (2011).
- 384 35. D. L. Moorhead, R. L. Sinsabaugh, A theoretical model of litter decay and  
385 microbial interaction. *Ecological Monographs* **76**, 151-174 (2006).
- 386 36. E. V. Blagodatskaya, S. A. Blagodatsky, T. H. Anderson, Y. Kuzyakov, Priming  
387 effects in Chernozem induced by glucose and N in relation to microbial growth  
388 strategies. *Applied Soil Ecology* **37**, 95-105 (2007).
- 389 37. M. P. Waldrop, D. R. Zak, R. L. Sinsabaugh, Microbial community response to  
390 nitrogen deposition in northern forest ecosystems. *Soil Biology and Biochemistry*  
391 **36**, 1443-1451 (2004).
- 392